INSPECTION OF THE SPACE SHUTTLE EXTERNAL TANK SOFI USING NEAR-FIELD AND FOCUSED MILLIMETER WAVE NONDESTRUCTIVE TESTING TECHNIQUES

S. Kharkovsky[1], F. Hepburn[2], J. Walker[2] and R. Zoughi[1]

[1]Applied Microwave Nondestructive Testing Laboratory (amntl)
Electrical and Computer Engineering Department
University of Missouri-Rolla
Rolla, Missouri 65409

[2]NASA George C. Marshall Space Flight Center
Marshall Space Flight Center, AL 35812

ABSTRACT

*The Space Shuttle Columbia's catastrophic failure has been attributed to a piece of external tank SOFI (**S**pray **O**n **F**oam **I**nsulation) striking the left wing of the orbiter causing significant damage to some of the reinforced carbon/carbon leading edge wing panels. Subsequently, several nondestructive testing (NDT) techniques have been considered for inspecting the external tank. One such method involves using millimeter waves which have been shown to easily penetrate through the foam and provide high resolution images of its interior structures. This paper presents the results of inspecting three different SOFI covered panels by reflectometers at millimeter wave frequencies, specifically at 100 GHz. Each panel was fitted with various embedded anomalies/inserts representing voids and unbonds of different shapes, sizes and locations within each panel. In conjunction with these reflectometers, radiators including a focused lens antenna and a small horn antenna were used. The focused lens antenna provided for a footprint diameter of approximately 1.25 cm (0.5") at 25.4 cm (10") away from the lens surface. The horn antenna was primarily operated in its near-field for obtaining relatively high resolution images. These images were produced using 2D scanning mechanisms. Discussions of the difference between the capabilities of these two types of antennas (radiators) for the purpose of inspecting the SOFI as it relates to the produced images are also presented.*

Keywords: *millimeter waves, near-field, insulating foam, SOFI, unbond, void, focusing lens, horn antenna.*

BACKGROUND

The Space Shuttle Columbia Accident Investigation Board (CAIB) report has pointed to a flyaway section of SOFI (**S**pray **O**n **F**oam **I**nsulation) from the left bipod fairing on the external fuel tank as the cause of bringing down the Space Shuttle Columbia during reentry into the atmosphere [1]. Some critical foam loss regions of the external tank are structurally complex in geometry and design. Therefore, any nondestructive testing (NDT) technique used for inspecting the state of the foam must be able to overcome many limiting issues that are brought upon by this complexity. Additionally, this insulating closed-cell foam material is by nature low density and may be as thick as 23 cm (9") in some regions of the tank which consequently presents many of the standard NDT techniques with significant challenges for a robust inspection. In the microwave and millimeter wave frequency ranges, the low density nature of the foam and its polymeric makeup translate to a low dielectric permittivity and loss factor. In other words, the difference between the dielectric properties of the foam and anomalies, such as voids or unbonds, is small. For example, the (relative-to-air) dielectric properties of a typical piece of SOFI was measured at 10 GHz to be (1.05 – j0.003) [2]. Subsequently, when using these frequencies, sensitive inspection systems must be carefully designed in such a way that the presence of these "weak scattering" anomalies can still be detected. An advantage of high frequency measurements is the inherent capability of obtaining high resolution images when imaging a structure. The well-established millimeter wave spectrum is 30 GHz – 300 GHz corresponding to a wavelength range of 10 mm – 1 mm [3]. Figure 1 shows the frequency and wavelengths associated with millimeter waves.

In the past, several NDT techniques have been attempted for this particular inspection purpose [4-5] including microwave and millimeter wave methods [6]. The microwave and millimeter wave methods were found to produce encouraging results which has led to further investigation of these techniques in particular at the higher millimeter wave frequencies. At these frequencies the signal propagates inside the foam without much attenuation so that thin as well as thick foam can be interrogated and there is still a reasonable and detectable distinction between the dielectric properties of the foam and anomalies rendering their presence detectable (i.e., sufficient scattered signal). Moreover, at these frequencies, probe dimensions (i.e., waveguides and antennas) are relatively small and when used in the near-field mode can produce images with relatively high

spatial resolution [7]. Finally, millimeter wave techniques utilizing focusing methods such as lens antennas provide for a compact and high resolution measurement system. In all cases, the measurement systems at these frequencies are small and are easily adaptable to existing scanning mechanisms. More importantly, since these techniques do not commonly utilize pulsing of the transmitted incident signal, there is no need for time gating or focusing the pulsed beam at a restrictively specific location within the structure [7]. These techniques utilize systems that irradiate the structure continuously and provide information about the state of the structure in a comprehensive manner (i.e., through foam depth or thickness). Consequently and when using focused techniques, images from anomalies at different depths within the structure may appear somewhat fuzzy (i.e., not focused), however they will not be missed, as will be seen later. This is an important attribute of these techniques.

Subsequent to the Space Shuttle Columbia's catastrophic failure, the NASA Marshall Space Flight Center embarked upon a program of evaluating all NDT techniques suitable for inspecting the SOFI. Near-field microwave and millimeter wave NDT methods were one of the techniques chosen for this purpose [2, 4-6]. This paper presents the results of inspecting several SOFI panels using robust millimeter wave techniques incorporating both near-field and focused measurement approaches.

MEASUREMENT APPROACH

A reflectometer system operating at 100 GHz, within the W-band (75 GHz – 110 GHz), and composed of a combined, or mono-static, transmitting and receiving millimeter wave sections was designed. In this way one antenna may be used for both transmitting and receiving the millimeter wave signal. Mono-static systems are compact and since they use only one antenna there is no need or requirement for proper alignment of the transmitting and receiving antennas. Here, the transmitted and received signals correspond to the same illuminated areas/volumes unlike a bi-static measurement system in which a separate transmitting and receiving antennas are required. Compared to a bi-static system in which the two antennas are sufficiently apart, the coupling of the transmitted and received signals in a mono-static system may reduce the system dynamic range. However, using high quality transmitter-receiver signal separators can provide for significant de-coupling between these two signals while maintaining a sufficiently high level

of measurement dynamic range. Careful design of such mono-static systems can also produce images that are phase and/or magnitude sensitive [2,7]. This is important since depending on the dielectric properties of the structure under inspection and the type of anomaly that may exist in the structure the phase or the magnitude of the reflected signal from an anomaly may be a better indicator of its presence and properties. Subsequently, both a small horn antenna and a focused lens antenna were used to produce images of several SOFI panels with various embedded anomalies representing voids and unbonds. The lens antenna had a focal length of 25.4 cm (10") with a corresponding footprint of 1.25 cm (0.5") at this distance. The small horn had aperture dimensions of 1 cm (0.4") by 1.4 cm (0.55") with a far-field operating distance of approximately 19.7 cm (7.75") corresponding to a footprint diameter of approximately 5 cm (2") at this distance [8]. Finally, when inspecting panels with stringers, images were produced using two distinct incident signal polarizations; namely, one in which the incident electric field polarization vector was parallel to the stringer axes (referred to as the parallel polarization) and one where this vector was perpendicular to the stringer axes (referred to as the perpendicular polarization). As will be seen later, polarization diversity which is a significant attribute of these millimeter wave measurements can provide images possessing different and complementary information about a particular anomaly when the anomaly is located near a structural member that has a preferred orientation with respect to the polarization vector direction. These structural members in this case include stringers, flanges, bolts, etc.

The panels were either placed on a computer-controlled 2D scanning table and the millimeter wave system was held at a certain distance above the panels or the system was attached to a 2D scanning mechanism held above the panel while the panel was scanned. Figure 2 shows a picture of the latter case with the millimeter wave system and the small horn antenna scanning one of the panels used in this investigation. It must be noted here that the input to the millimeter wave system is a DC voltage applied to a tunable Gunn oscillator and the system output is also a DC voltage proportional to the reflected phase and/or magnitude from the structure under inspection. Given the sensitivity and rise time associated with the detector, relatively fast scanning rates can be accommodated (i.e., in excess of linear 5 cm (2") per second). Subsequently, as the panel is scanned, the system output voltage is used to produce a raster scan or a 2D image of the panel. The measured output voltages are then normalized and assigned

different grayscale or color levels producing a grayscale or color image, respectively. It is important to note that by normalizing the images, the grayscale/color levels in one image do not necessarily correspond to the same output voltage levels in another image.

SOFI SAMPLES

Several panels were used in this study. The results for three specific panels are presented in this paper. These panels collectively provided for different and important geometries related to the complex structural properties of the External Tank as well as different types of anomalies that may be encountered.

Panel #1

Figure 3 shows the picture of panel #1. This panel consisted of a 55 cm (21.7") by 55 cm (21.7") and 10 cm (4") thick section of SOFI on to a flat 0.90 cm (0.35") thick aluminum substrate. However, the SOFI was not directly adhered to the substrate. The substrate was first covered with a relatively thin layer of super light ablator (SLA). Two square-shaped unbonds with side dimensions of 10 cm (4") and 5 cm (2") were produced using Teflon tape placed in between the aluminum substrate and the SLA layer. Four cubical voids, with respective side dimensions of 2.54 cm (1"), 1.9 cm (0.75"), 1.25 cm (0.5") and 0.63 cm (0.25"), were cut out of pieces of foam and were placed directly on top of the SLA layer. Each void was produced by hollowing out a cube of foam, which was then placed on the SLA layer prior to spraying the foam. A "rollover void" was also generated on top of the SLA layer. In practice this type of void may be introduced in areas where there is a significant change in the geometry of the tank, such as around bolts, stringers and flanges. During the spray-on foam process, if great care is not taken, the foam can roll over along an edge as it expands producing a pocket which can be trapped by the next pass of the foam spray if the liquid foam is not forced into the pocket. Finally, an unbond was produced using a thin layer of foam that was adhered to the SLA with four small drops of adhesive at its corners [6]. Figure 4 shows the schematic of this panel.

Panel #2

Panel #2 was designed to resemble the intertank flange portion of the fuel tank and consisted of three stringers, a flange and three bolts through the flange centered in front of the stringer

openings. The aluminum substrate thickness was 0.63 cm (0.25"). Figure 5 shows a picture of this panel prior to the application of the SOFI. Defects, rubber inserts and SOFI void inserts, were placed at several critical regions of this panel, as shown in Figure 5. The rubber anomalies are not expected to be found in an External Tank structure and were used here only for comparative purposes with the SOFI voids. Additionally, the foam inserts had circular cross-sections whereas the rubber inserts were square shaped. The SOFI was subsequently sprayed on this panel and the foam surface was then trimmed in a manner similar to the External Tank intertank flange close-out. Consequently, this panel possessed foam thickness ranging from 2.54 cm (1") to 10 cm (4") over different regions. Additionally, the foam on the top portion of the panel was in the form of a ramp which varied in thickness from 7.62 cm (3") to about 0.31 cm (0.125"). Figure 6 shows a picture of this panel.

Panel #3

Panel #3 consisted of a 55 cm (21.7") by 55 cm (21.7") by 20.32 cm (8") thick SOFI block on top of an aluminum substrate with a thickness of 0.32 cm (0.125"). As a result of the relatively thick foam on this panel and the thin substrate, the four corners of the substrate were lifted up during the cure of the SOFI causing the substrate to have an approximate concave (i.e., a shallow bowl) shape. Figure 7 shows a side view picture of this panel indicating this fact. Two sets of anomalies composed of voids and unbonds with different sizes and shapes were embedded in this panel. One set was placed directly on top of the substrate while the other set was placed halfway up in the foam thickness (e.g., 10 cm (4") above the substrate). Figure 8 shows the schematic of these embedded anomalies indicating their sizes and shapes. Two special voids (5 cm (2") in sides) were formed to test the ability of the inspection method to detect details within the void insert. These voids are labeled "little and big diagonal" and were formed by cutting a narrow (little) or wide (big) diagonal channel in the foam insert. This panel allowed evaluation of the capabilities of the millimeter wave system as a function of anomaly type, size and geometry as well as depth within a relatively thick SOFI structure.

RESULTS

Panel #1

A 40 cm (15.7") by 40 cm (15.7") area of panel #1 was scanned using the lens and the small horn antennas, as shown in Figures 9 and 10, respectively. In Figure 9 the distance between the surface of the substrate and the lens was 25.4 cm (10"). In this image all eight anomalies are clearly detected. The square shape associated with all of these anomalies are also clearly indicated in the image. Four distinct bright spots are seen at the four corners of the unbond located at the lower left corner. These spots correspond to four small drops of adhesive that were used to adhere the unbond insert to the SLA surface. The dimensions associated with each anomaly in the image are very close to their actual dimensions. Throughout this image several superimposed diagonal lines are seen as well. These correspond to regions of the foam with slightly higher density and subsequently different dielectric properties.

Figure 10 shows the image of this panel when the distance between the small horn aperture and the top surface of the foam sample was 0.6 cm (0.24"), putting the horn aperture distance to the top of the substrate at 10.6 cm (4.17"). When comparing the images in Figures 9 and 10, one can see much similarity between them. The dimensions of the embedded anomalies associated with their images closely correspond to their actual dimensions. Except for the upper central regions of the image, for the most part this image is more clear and sharp than the one shown in Figure 9. The four small drops of adhesive and the boundaries of the unbond associated with them are clearly visible in this image.

In both images of this panel there are several indications (i.e., three around the upper right unbond). These may be due to the presence of small natural voids that may have been produced during the manufacturing of this panel. This fact may be validated in the future when and if this panel is dissected or imaged with a higher resolution system (intended future work).

Panel #2

One of the attractive features of millimeter wave measurement techniques using linearly polarized irradiating waves is the fact that the relative orientation of the polarization vector and

prominent structural features, such as stringers and flanges, can be manipulated to reduce unwanted reflections and increase sensitivity to desired features. Polarization diversity, or the use of two orthogonal polarizations has been effectively demonstrated for this purpose in the past [6]. Similarly, two orthogonal polarizations were used in this investigation when inspecting panel #2. This panel possessed structural attributes that rendered the use of two orthogonal polarizations useful. The other two panels possessed structural and anomaly geometries that would produce similar images when using two orthogonal signal polarizations.

Parallel Polarization with Lens Antenna

Figure 11 shows the image of this panel using the lens antenna at a distance of 25.4 cm (10") from the substrate with the polarization vector parallel to the stringer axes. Due to the scanning size limitation associated with the scanning table, this image is a composite of four separate images that are augmented to produce the final image. The results clearly indicate the detailed structural features of the panel when compared to its picture shown in Figure 5. The three stringers, the flange, the three bolts through the flange, the bolts along the stringers, the stringer opening and the cut foam pattern between the stringers (see Figure 6) are all clearly visible in this image.

The two sets of three square rubber inserts and round foam void inserts are also clearly detected at the top of the image. The square shape of the rubber inserts (particularly the largest one) and the round shape of the foam voids can easily be deciphered from their respective images.

The flange is also clearly detected in addition to a long indication in the middle of the flange. This is the indication of the boundary between the two separate pieces of aluminum that are bolted together to produce the flange. The three bolts through the flange are also distinctly shown. The rubber and foam inserts under the bolt heads are not separately detected. However, a closer inspection of the bolt head images reveals that the bolt head with the rubber insert extending out from under it (on the left) has a wider image that the one with a small foam insert under it (on the right). The same is also true for the middle bolt head. On the other hand, there is no real indication of the rubber insert under the nut (on the left) when its image is compared with the other two nuts.

The two rubber inserts between the left and the middle stringers are detected since the rubber dielectric properties are more substantially different than the foam as compared to air and foam. The voids between the middle and the right stringers can barely be seen in the image with the smaller void having a much fainter intensity in the image (this void can be seen better in later images). The same can also be said for the rubber and foam inserts on the tops of the middle and right stringers. The rubber and foam inserts on the sides of these two stringers are not detected in this image. It must be noted that an additional and unexpected indication was detected between the upper portions of the middle and the right stringers, marked with the dashed square in Figure 11. This indication was more prominently detected using the small horn antenna, as will be shown later. It is believed that this is the indication of the presence of a natural void that was produced during the manufacturing of the panel. This fact may be verified by dissecting the foam to reveal the presence of this void. In the future we plan on imaging this panel at higher millimeter wave frequencies which should give more information about the nature of this indication.

Finally, one can clearly see indications in the centers of all three stringer openings (the dark curved features). However, a foam void was placed in the right stringer opening region and none in the other two. As a matter of fact the indication in the middle stringer opening is the strongest of all three. It turns out that during the manufacturing of this panel, three cavities were unintentionally produced in the foam directly above these three stringer opening areas. Additionally, the cavities in all three regions possess a distinct curved shape. Figure 12 shows a close up picture of the foam surface indicating these three cavities.

Perpendicular Polarization with Lens Antenna

Figure 13 shows the image of this panel using the lens antenna at a distance of 25.4 cm (10") from the substrate with the polarization vector perpendicular to the stringer axes. Due to the scanning size limitation associated with the scanning table, this image is a composite of four separate images that are augmented to produce the final image. The bright line through the middle stringer and the slight misalignment in the middle of the flange and the bolt at this location are an artifact of augmenting these four images and is not an indication of embedded

anomalies. Similar to the image shown in Figure 11, with the exception of the inserts on the sides of the stringers and those under the flange bolts, all other inserts are detected, at least to some degree. The foam void between the middle and the right stringers are more clearly detected in this image. This is not a polarization effect and most likely has to do with the arrangement of the panel prior to imaging this section.

When compared to Figure 11, it is clear that at this polarization the images of the flange areas are clearer, revealing more of its structural detail. One may also see more indications of the inserts as they extend out from under the flange bolts at this polarization. The stringer opening regions are more vivid in this image as well. In this image, the horizontal terminating edge at the top of the stringers is somewhat more distinctly detected.

Parallel Polarization with Horn Antenna

Figure 14 shows the image of this panel using the horn antenna at a distance of 10.5 cm (4.13") from the substrate with the polarization vector parallel to the stringer axes. This image is a composite of four separate images that are augmented to produce the final image. The line through the image and in the middle of the left and the middle stringers is an artifact of augmenting these four images and is not an indication of an embedded anomaly. This image shows all of the anomalies and features that were shown in the images using the lens antenna (Figure 11). However, due to the fact that during the scan some of the inserts and anomalies were at different distances from the horn aperture (in its near-field region), their indications are much more distinct than those in Figure 11. Examples of these are the foam inserts on top of the right stringer in which even the smaller foam insert is clearly detected and the foam inserts between the middle and the right stringers which shows the smaller foam insert better than its counterpart in Figure 11. The presence of the unintended void in the upper portion of the region between the middle and the right stringers is also more strongly sensed (shown by the dashed square). The stringer opening regions have a clearer image with the horn than with the lens. The strong indication in the center of the right stringer opening is due to the presence of the foam void placed there (see Figure 5) in addition to the natural cavity in the foam at this location. The presence of the cavities in the foam at the other two stringer openings is also detected but more consistent with the size and features of these respective voided regions (see Figure 12). The

square shape associated with the rubber inserts and the round shapes associated with the foam inserts in the top region of the panel are more clearly illustrated in this image than those using the lens antenna. Finally, it may also be argued that the presence of the rubber insert extending out from under the flange bolt caused more signal perturbation using the horn antenna than when using the lens antenna.

Similar to the two previous images of this panel, the presence of the rubber inserts and foam voids on the sides of the stringers was not detected with the horn antenna either. The stringer bolts were not as distinctly detected using the horn antenna since at that distance the spatial resolution associated with the antenna footprint is larger than that with the lens antenna.

Perpendicular Polarization with Horn Antenna

Figure 15 shows the image of this panel using the horn antenna at a distance of 10.5 cm (4.13") from the substrate with the polarization vector perpendicular to the stringer axes. As in the previous case, many of the embedded inserts are clearly detected at this polarization. However, overall this image is less clear than its parallel polarization counterpart. The stringer opening regions do not clearly indicate distinct presence of the voids (embedded and natural) in the order of sizes they actually are.

Overall, the inspection of this more realistic panel was quite successful using these two antennas and implementing polarization diversity. More detailed and collective discussion of the results will be given in the Discussions section.

Panel #3

Figure 16 shows the image of this panel using the lens antenna at a distance of 45.7 cm (18") from the substrate. This distance was used in this case since it produced better images of this panel. All of the embedded inserts at the substrate (as shown in Figure 8) corresponding to the top half of the image are distinctly detected showing their relative sizes. Moreover, the hollowness associated with the voids is visible through the slight shadows (i.e., the dark boundary indications) produced due to the fact that the corners of the panel were lifted up, as explained earlier (see Figure 7). The rings and halos around the voids and the unbonds are due

to the fact that that at this distance the influence of the radiating beam sidelobes may have been more significant than at its designed focal length. The "big diagonal" void in lower left corner of this section is also clearly detected.

With the exception of three unbonds, the rest of the inserts are also detected when placed in the middle of the panel depth corresponding to the lower half of the image. It should be noted that the 1" and the 0.5" voids are shifted with respect to their positions shown in the schematic (see Figure 8) due to a manufacturing error. The three unbonds may at least be partially masked by the prominent rings, fringes, in this image, in particular in the lower right corner, which are artifacts of interference effects caused by the raised corners of the substrate. Consequently, the distance between the lens and the substrate varied throughout the sample producing these rings. The "little diagonal" void in the lower left corner of the image, is also detected.

Figure 17 shows the image of this panel (composite of four separate images) using the horn antenna at a distance of 20.9 cm (8.24") from the substrate. At this distance the footprint associated with this horn is substantially larger than that of the lens resulting in an image with an expectedly degraded spatial resolution. This fact is clearly shown in this image since primarily only the larger voids are detected. The larger unbonds at the substrate are detected but not those placed in the middle of the foam thickness. Some weak indication of the "big diagonal" void can be seen in this image but not of the "little diagonal" void. The superimposed ring pattern is also shown in this image due to interference effects caused by the raised corners of the panel. Overall, the results for this panel, when using the horn antenna, are not as good as when using the lens antenna due to better focusing capabilities of the lens.

DISCUSSION

The results of this investigation clearly points to the effective utility of millimeter wave nondestructive testing (NDT) techniques for inspecting the Space Shuttle External Tank SOFI. Millimeter wave signals easily penetrate through the foam and sense anomalies and discontinuities. The measurement system consisted of a W-band (75 GHz - 110 GHz) mono-static reflectometer operating at 100 GHz. The radiators for this system consisted of a focused lens antenna and a small horn antenna which was primarily operated in its near-field region.

Each of these techniques resulted in informative images of the three investigated panels. These three panels collectively provided for different and important geometries related to the complex structural features of the External Tank and different types of discontinuities and anomalies which may be found within the SOFI. It was shown that once an anomaly is detected, its spatial dimensions obtained from its image closely correspond to its actual dimensions. The images of voids consistently possessed features that distinguished them from unbonds (i.e., shadows). Most inserts placed on or near the substrates were readily detected. However, a few thin foam unbond inserts placed in middle of a foam thickness were not readily detected. In many of these cases unwanted signals, such as interference fringes, rings, in an image due to a warp in the substrate, masked the indication of these subtle inserts. The images produced from panel #2 revealed the structural details of the panel such as the flange, stringers, bolts, etc. The images of the regions associated with the stringer openings clearly produced indications of unwanted anomalies and natural cavities there. It turned out that besides the one foam voids cube placed in one of the stringer openings, all three had cavities in the foam covering those regions.

Polarization diversity is an important feature of these techniques. It was shown that using two orthogonal polarizations can yield additional and complementary information that can be used to more accurately evaluate the interior state of the SOFI near structural details with complex geometry (e.g., stringers, flange, bolts, etc.). This leads to the fact that overall, these techniques are very robust and the reflectometer systems are rugged and have an extremely high degree of repeatability. Repeatability of the system was not specifically discussed here. However, it must be mentioned that throughout this investigation multiple (similar) measurements on a panel resulted in images with the same information content. Using small horns that provide for some degree of focusing compared to open-ended waveguides, in addition to the fact that when operating in their near-field region the resulting spatial resolution is primarily a function of the horn aperture dimensions, rendered images that better exposed some of the inserts compared to the lens antenna. The lens antenna also consistently produced high resolution images, and it provided better images of anomalies placed inside of thick foam. The perimeters or boundaries of the inserts were consistently better detected using the lens primarily due to its narrow and well-defined beam pattern. Moreover, features associated with internal geometries of some of the foam voids such as the diagonals were also detected. Inserts at the sides of the stringers were

not robustly detected using either antenna. Efforts are being expanded to modify the measurement approach to render these inserts detectable as well.

Since these reflectometer systems use continuous wave (CW) and do not use pulsed methods there is no need for time gating. Hence, once an image is produced it provides through thickness information. This is important since whether using a lens or a small horn detectable anomalies, through the depth, will be detected. If necessary, one may subsequently use various approaches to hone in on a particular depth to obtain a clearer image from that depth. This may be accomplished using the focused method or alternatively using signal processing methods. Finally, it must be mentioned that all the images shown in this paper were raw images and no signal processing was applied to them to enhance their information or image contents. The outcome of this investigation is very positive and encouraging and as the technology is further expanded and improved these rugged and robust millimeter wave reflectometer systems will continue to provide more encouraging and useful results.

Acknowledgement: This work was supported through a cooperative agreement from the NASA George C. Marshall Space Flight Center in Huntsville, Alabama.

REFERENCES

1. Columbia Accident Investigation Board Report, NASA, August 2003.
2. Shrestha S., S. Kharkovsky, R. Zoughi, F.L. Hepburn and G. Workman, "Microwave Nondestructive Inspection of Thick Insulating Foam," *The American Society for Non-Destructive Testing (ASNT) Fall Conference and Quality Testing Show*, Pittsburgh, PA, 13-17 October 2003.
3. Pozar, D.M., *Microwave Engineering*, 2nd Edition, Addison Wesley Publishing Co., Inc., NY, NY, 1990.
4. Davis C., F. Santos, "Shearography NDE of Space Launch Vehicles," *The American Society for Non-Destructive Testing (ASNT) Fall Conference and Quality Testing Show*, Pittsburgh, PA, 13-17 October 2003.
5. Madaras E., "Terahertz NDE for Inspection of Shuttle Foam," *The American Society for Non-Destructive Testing (ASNT) Fall Conference and Quality Testing Show*, Pittsburgh, PA, 13-17 October 2003.
6. Shrestha S., S. Kharkovsky, R. Zoughi, F.L. Hepburn, "Microwave and Millimeter Wave Nondestructive Evaluation of the External Tank Insulating Foam," *Materials Evaluation*, March 2005.
7. Zoughi, R., *Microwave Non-Destructive Testing and Evaluation*, Kluwer Academic Publishers, The Netherlands, 2000.
8. Balanis, C.A., Antenna Theory: Analysis and Design, 2nd Edition, John Wiley and Sons, NY, NY, 1997.

List of Figures

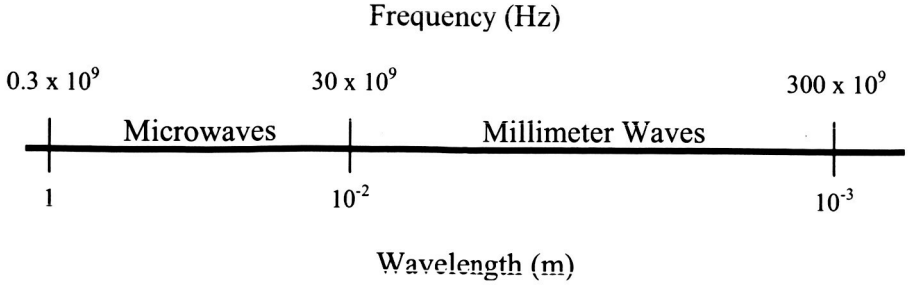

Figure 1

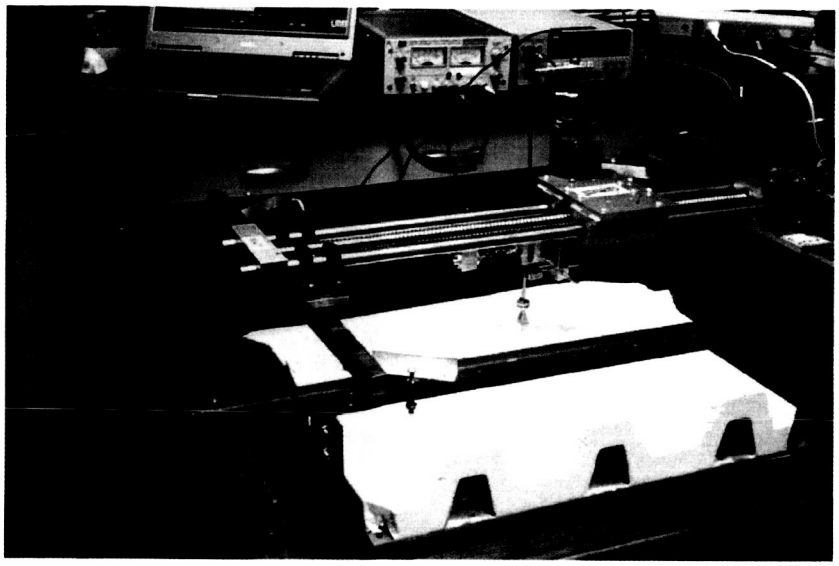

Figure 2

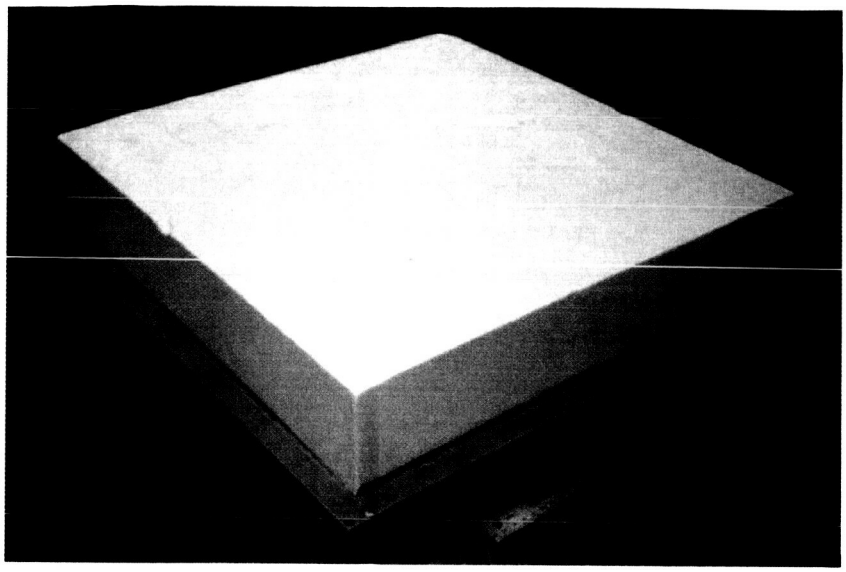

Figure 3

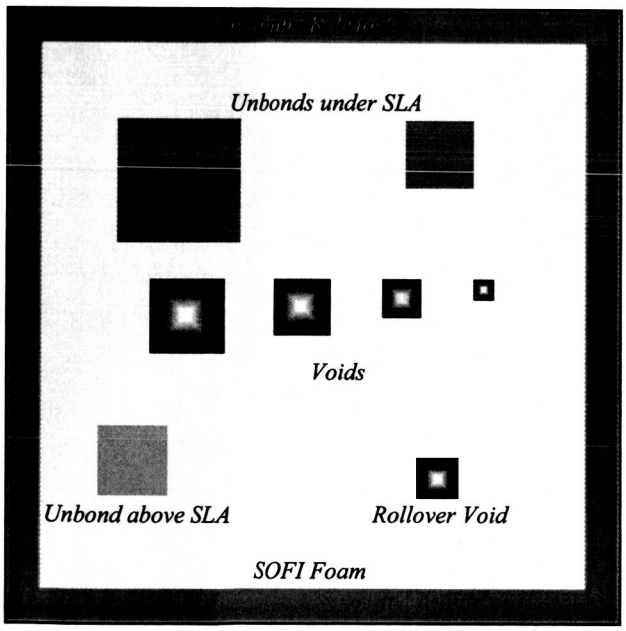

Figure 4

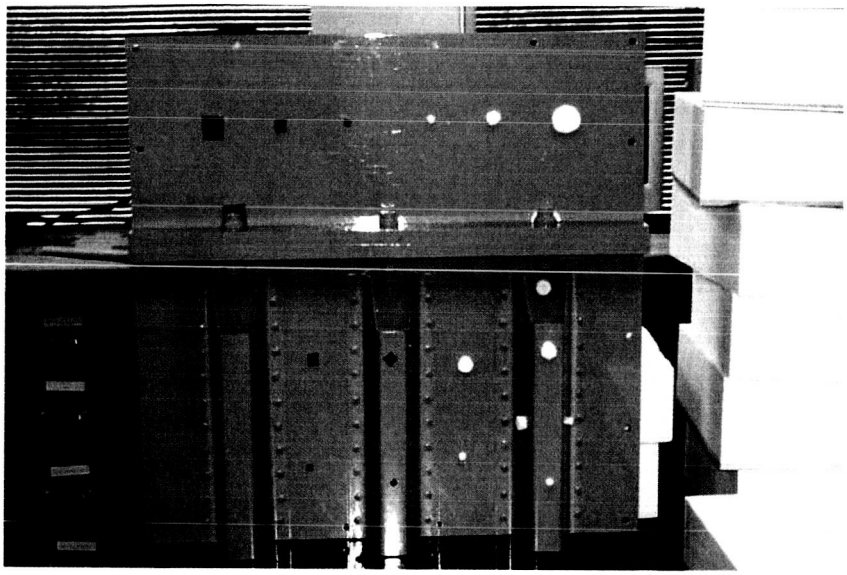

Figure 5

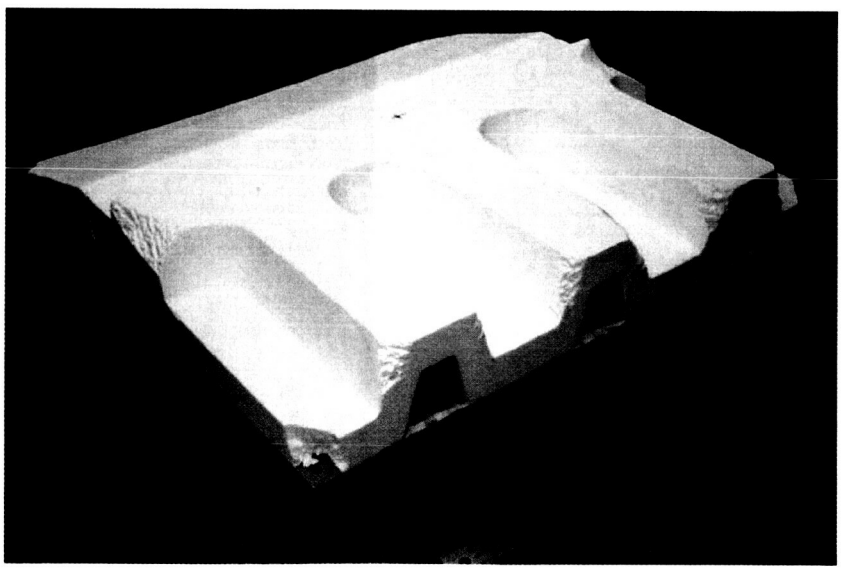

Figure 6

Figure 7

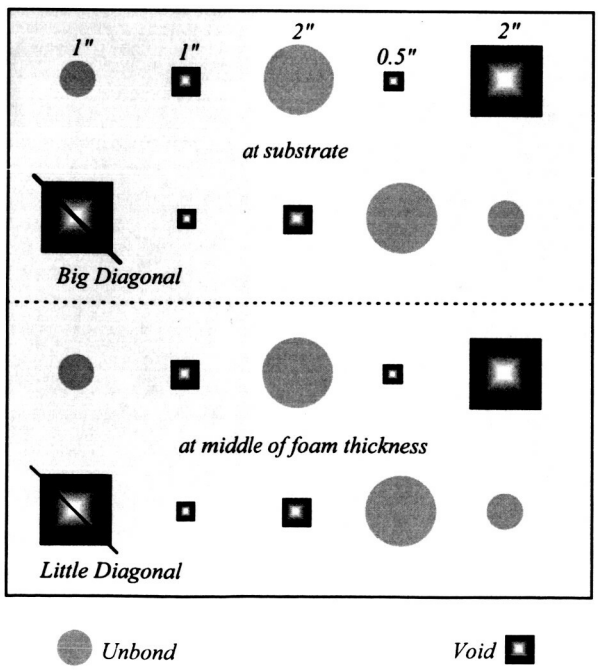

Figure 8

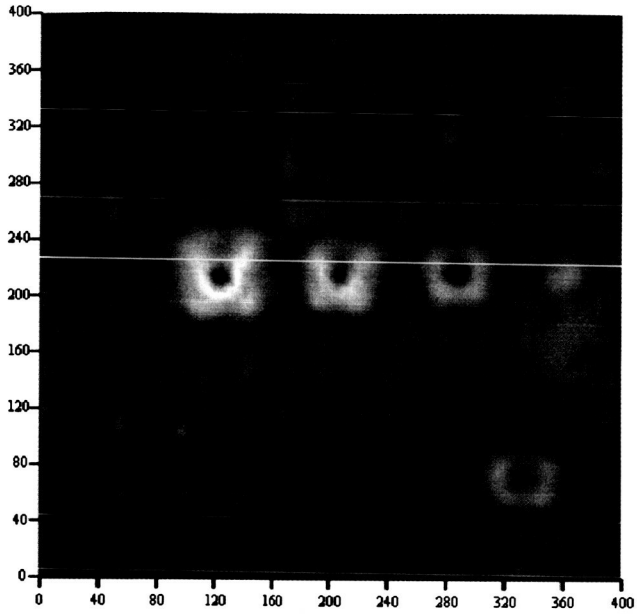

Figure 9

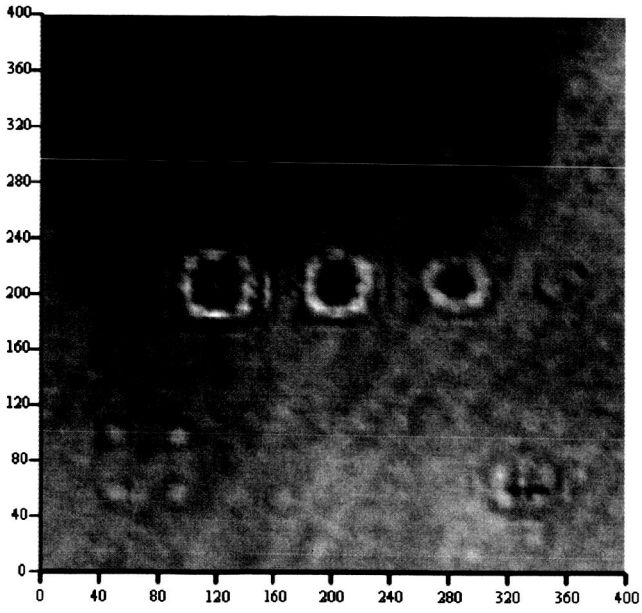

Figure 10

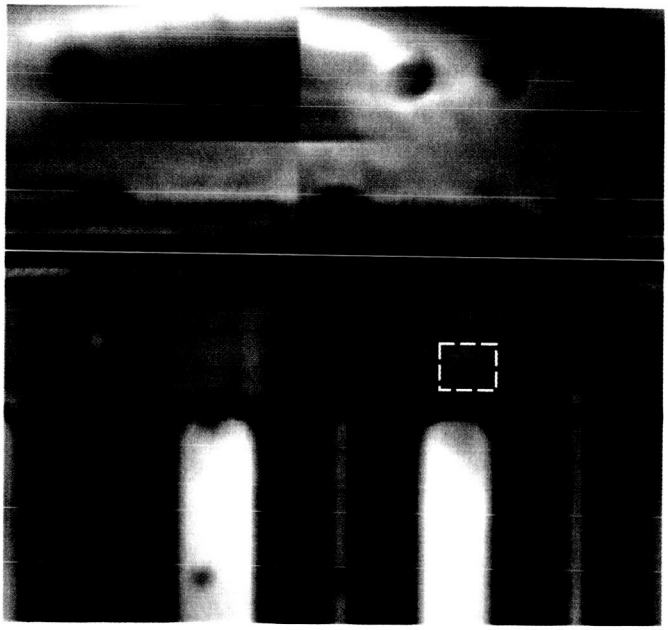

Figure 11

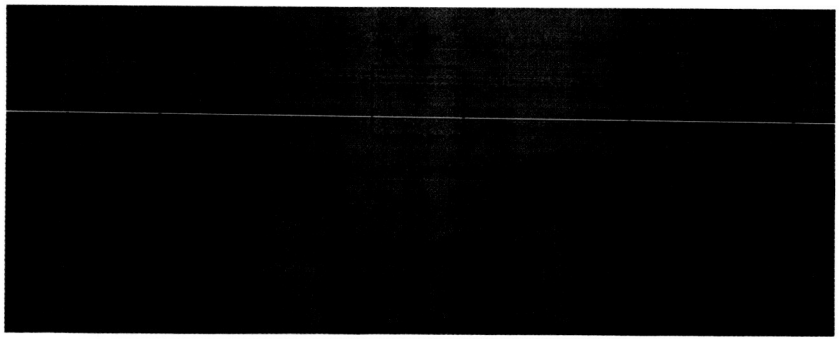

Figure 12

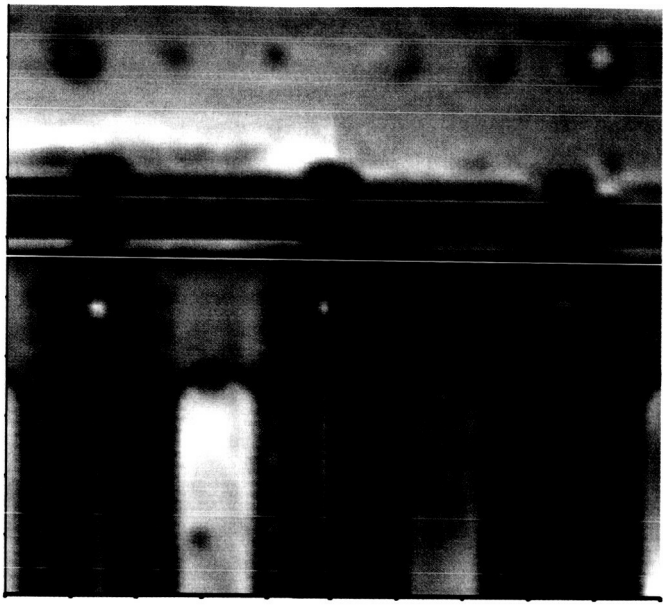

Figure 13

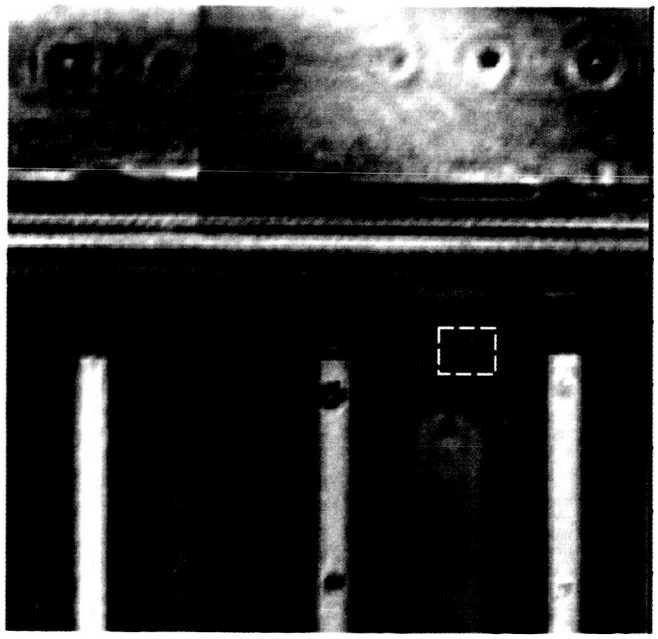

Figure 14

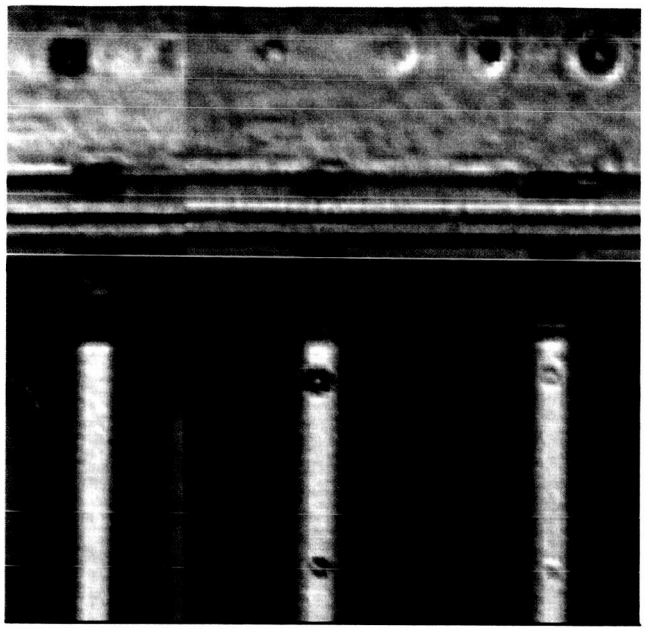

Figure 15

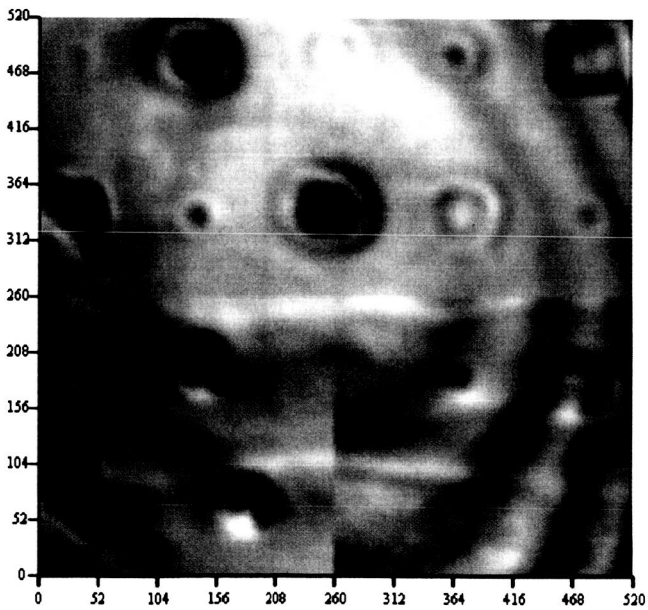

Figure 16

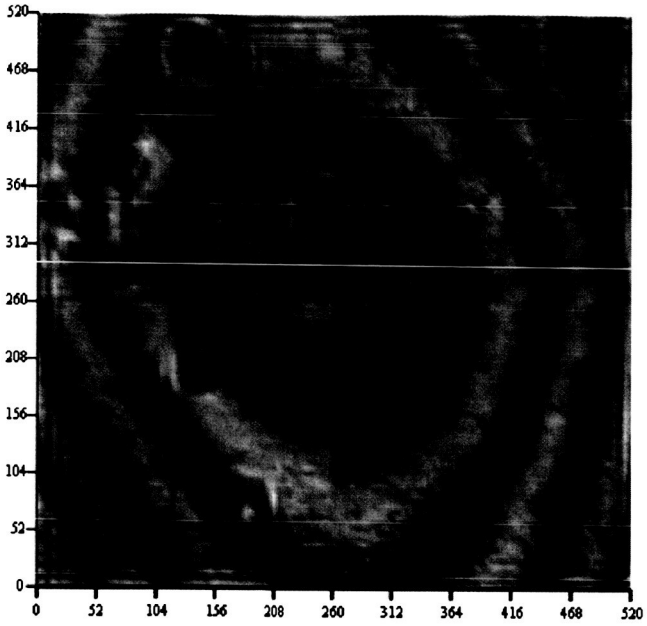
520
468
416
364
312
260
208
156
104
52
0
0
52
104
156
208
260
312
364
416
468
520

Figure 17